Disentangling bulk and surface Rashba effects in ferroelectric α-GeTe

J. Krempaský,[1] H. Volfová,[2] S. Muff,[1,3] N. Pilet,[1] G. Landolt,[1,4] M. Radović,[1,5] M. Shi,[1] D. Kriegner,[6] V. Holý,[6] J. Braun,[2] H. Ebert,[2] F. Bisti,[1] V. A. Rogalev,[1] V. N. Strocov,[1] G. Springholz,[7] J. Minár,[2,8] and J. H. Dil[1,3]

[1]*Swiss Light Source, Paul Scherrer Institut, CH-5232 Villigen PSI, Switzerland*

[2]*Department of Chemistry, Ludwig Maximillian University, 81377 Munich, Germany*

[3]*Institute of physics, Ecole Polytechnique Fédérale de Lausanne, CH-1015 Lausanne, Switzerland*

[4]*Physik-Institut, Universität Zürich, Winterthurerstrasse 190, 8057 Zürich, Switzerland*

[5]*SwissFEL, Paul Scherrer Institut, CH-5232 Villigen PSI, Switzerland*

[6]*Department of Condensed Matter Physics, Charles University, Ke Karlovu 5, 121 16 Praha 2, Czech Republic*

[7]*Institut für Halbleiter-und Festkörperphysik, Johannes Kepler Universität, A-4040 Linz, Austria*

[8]*New Technologies-Research Center University of West Bohemia, Plzeň, Czech Republic*

(Received 25 May 2016; revised manuscript received 5 October 2016; published 7 November 2016)

Macroscopic ferroelectric order in α-GeTe with its noncentrosymmetric lattice structure leads to a giant Rashba spin splitting in the bulk bands due to strong spin-orbit interaction. Direct measurements of the bulk band structure using soft x-ray angle-resolved photoemission (ARPES) reveals the three-dimensional electronic structure with spindle torus shape. By combining high-resolution and spin-resolved ARPES as well as photoemission calculations, the bulk electronic structure is disentangled from the two-dimensional surface electronic structure by means of surface capping, which quenches the complex surface electronic structure. This unravels the bulk Rashba-split states in the ferroelectric Rashba α-GeTe(111) semiconductor exhibiting a giant spin splitting with Rashba parameter α_R around 4.2 eV Å, the highest of so-far known materials.

DOI: 10.1103/PhysRevB.94.205111

In spintronics an important goal is to be able to control the spin of the electron in solids without applying magnetic fields [1,2]. The most promising mechanism is based on the Rashba effect [3] and the subsequent spin precession induced in such systems [4]. While most research has previously focused on 2D electron systems [5,6], recently a three-dimensional (3D) form of such Rashba effect was found in a series of bismuth tellurohalides BiTeX (X = I, Br, or Cl) [7–12]. Although these materials exhibit a very large spin splitting, they lack an important property concerning functionalization, namely, the possibility to switch or tune the spin texture. This limitation can be overcome in a new class of functional materials displaying Rashba splitting coupled to ferroelectricity, the so-called ferroelectric Rashba semiconductors (FERS) [13,14].

Recent photoemission experiments on α-GeTe—the stable rhombohedral room temperature configuration of the GeTe phase change material [15]—indicate that this system is a hallmark candidate for entanglement of the ferroelectric and spin-orbit order [16,17]. Due to the giant Rashba splitting spin injection from magnetic systems into GeTe appears viable in order to achieve spin-to-charge conversion [18]. Therefore, ferroelectric [13] or multiferroic [19] Rashba semiconductors bring new multifunctional assets for spintronic devices. A crucial issue for the understanding of FERS is to disentangle the Rashba effect in the bulk caused by the bulk ferroelectric lattice distortion and surface effects arising from particular surface terminations and/or possible band bendings. This represents a major challenge for surface sensitive techniques such as angle-resolved photoemission (ARPES). For this reason up to now ARPES measurements on α-GeTe surfaces performed in the surface-sensitive UV regime have been dominated by surface effects [16,17] and clear information of the three-dimensional bulk electronic structure and its spin texture has not been obtained.

In this paper, we demonstrate direct measurements of the bulk band electronic structure of α-GeTe using ARPES in the soft x-ray regime and elucidate the spindle torus shape of the bulk constant-energy surfaces that are further characterized by spin-resolved ARPES (SARPES) in the ultraviolet regime. We show that the α-GeTe(111) surface exhibits a multitude of the surface and resonantly enhanced bulk states at the Fermi level that induces conductivity in the otherwise semiconducting α-GeTe thin films. In particular, we reveal that the previously reported bulklike Rashba state [16] is actually a surface resonance and thus cannot contribute to spin-charge conversion in realistic devices [18]. Quenching of these states is demonstrated by amorphous tellurium capping of the GeTe surface rendering data dominated by bulk effects. The availability of gapped Rashba-split bands with their spin helicity locked to the direction of the ferroelectric polarization, as well as the immunity of these states to capping layers, paves the way to all-electric nonvolatile control of spin-transport properties in heterostructure α-GeTe based semiconductor devices.

The measurements were performed at the Swiss Light Source of the Paul Scherrer Institut. The soft x-ray ARPES data were taken at the ADRESS beam line at photon energies of 340–800 eV at a sample temperature of 11 K and a base pressure lower than 10^{-10} mbar [20]. The SARPES data were measured with the Mott polarimeters at the COPHEE end station at 20 K [21]. Experiments were performed on 200-nm-thick ferroelectric Te-terminated α-GeTe(111) films (see Supplemental Material [22]) grown by molecular beam epitaxy on BaF_2(111) substrates [19,23]. A protective stack of amorphous Te- and Se-capping layers with a total thickness of 20 nm was used to avoid surface degradation and oxidation. A complete or partial removal of the protective Te/Se stack in the ultrahigh vacuum chamber was achieved by annealing at different temperatures [22]. To build a bridge between

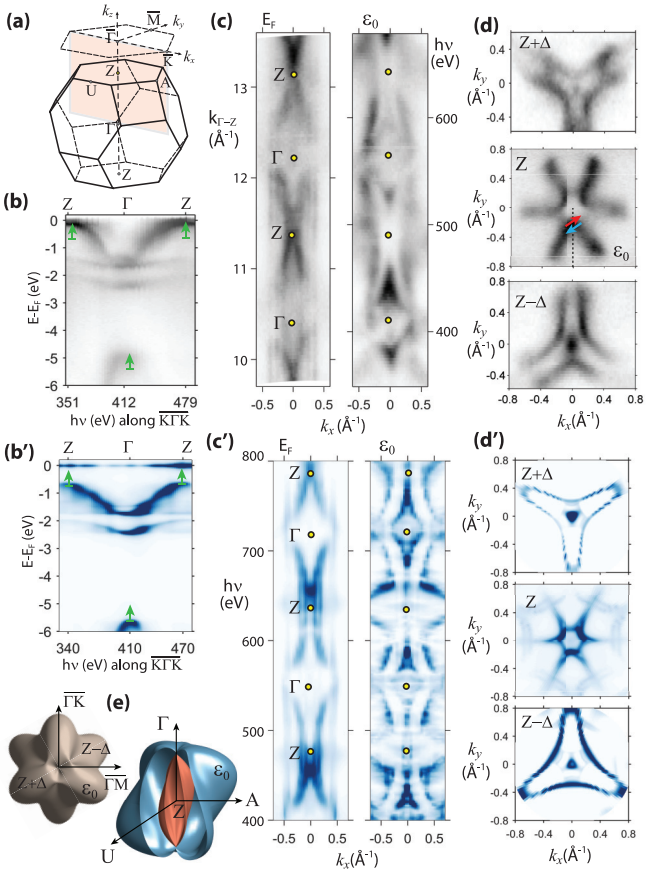

FIG. 1. (a) Brillouin zone of quasicubic GeTe. (b) k_z ARPES band maps along $Z\Gamma Z$ in normal emission and (c) $\overline{K\Gamma K}$ direction at E_F and $\epsilon_0 = 0.7$ eV binding energy; (d) constant binding energy maps above $(Z + \Delta)$, below $(Z - \Delta)$ and at the Z point. (b′), (c′), (d′) 1SM calculations corresponding to (b), (c), (d). (e) 3D schematic representation of the bulk isoenergy surface at ϵ_0.

experiment and theory our *ab initio* calculations are based on density functional theory as implemented within the multiple scattering theory including the spin-orbit coupling (SOC) [24,25]. The ground state band structures are presented in terms of Bloch spectral functions (BSF) and compared to final states by means of the one-step ARPES model (1SM), both include the intrinsic p-type doping due to Ge vacancies by means of coherent potential approximation alloy theory.

We first concentrate on locating the Z point in **k** space where the Rashba splitting is most pronounced. Figure 1 summarizes our data obtained with photon energies from 340 to 800 eV from uncapped surfaces. The experimental band maps are shown in panels (b)–(d), and the corresponding (b′)–(d′) panels with blue color scale are the photoemission calculations. A fundamental advantage of this energy range is the increase of the photoelectron escape depth and thus of intrinsic definition of the ARPES experiment in surface-perpendicular momentum $k_\perp$ which is crucial for observation of the inherently 3D electronic structure of α-GeTe(111) [26]. This is revealed by normal emission data as a function of $k_\perp$ varied through photon energy [panels (b)–(b′)] and by the dispersive spectral weight at the Fermi level (E_F) and at a binding energy of 700 meV (c–c′), readily identifying the Z points in the 3D Brillouin zone. The constant energy surface maps in (d)–(d′) show a strong hexagonal warping, which becomes threefold away from the Z points. In accordance with the crystal symmetry, these band maps are consistent with the 3D Rashba-type Fermi surface for BiTeI [8], taking the form of a spin-polarized spindle torus as depicted in panel (e).

Measured at the Z point at $h\nu = 480$ eV and at the Γ point at $h\nu = 410$ eV, ARPES data along the $\overline{K\Gamma K}$ direction for amorphous Te-capped and uncapped samples are shown in Figs. 2(c)–2(f), along with corresponding ground-state calculations (a), (b). Apart from the typical underestimate of the bandwidth and gap size, the calculations reproduce the experimental α-GeTe(111) bulk electronic structure very well because all the main bands 1-2-3 are unambiguously resolved in both theory and experiment. We emphasize that at the Γ point even the bulk Rashba splitting is experimentally resolved for bands 2 and 3. At the Z point it becomes evident that the uncapped surface in Figs. 2(c) and 2(d) unleashes otherwise suppressed surface effects on top of a bulklike electronic structure. As seen in Figs. 1(c) and 1(c′), at the Fermi level both theory and experiment identify pure surface effects as nondispersive bands denoted $S_{1,2}$ in Fig. 2(c), together with dispersive surface effects we henceforth denote as surface resonances SR. The surface resonances in semiconductors typically fill the band gap and hybridize with the bulk states. As a matter of fact Fig. 2(d) indicates that the SR split off from the bulk band 1 and extend up to E_F.

To better characterize the surface electronic structure near the Z point where the Rashba splitting is most pronounced and, at the same time, most shadowed by surface states and resonances, Fig. 3 zooms into the smaller band-map window indicated by yellow frame in Fig. 2(e). In particular, the bulk ground state calculations in panel Fig. 3(d) are compared to semi-infinite surface calculations in panel (f). The corresponding ARPES data in panels (c) and (e) consistently show a modified band structure with 2D Rashba-split surface states $S_{1,2}$ that intersect the bulklike states, as schematically illustrated in Fig. 3(a) by yellow contours. For both Te-capped and uncapped samples the Dirac point is situated at around 200–250 meV binding energy. Moreover, its dispersion along the ΓZ-direction shown in Fig. 1(b) and 1(b′) is in agreement with *ab initio* calculations with [13] or without [27] SOC. ARPES data from Te-capped samples [Fig. 3(c)] clearly show the pair of Rashba-split bands at the Z point consistent with the band map sketched in Fig. 3(b). The well-resolved Rashba-split bulk bands allow us to derive the momentum splitting $\Delta k_R \approx 0.13$ Å^{-1}, an energy splitting $E_R \approx 190$ meV, and Rashba parameter α_R along the Z-A-direction to be around 4.2 eVÅ. Such a giant Rashba splitting even surpasses systems such as Bi/Ag(111) [28] and BiTeI [7,8] and is in excellent agreement with theoretical predictions [14].

A particularly interesting feature for potential spintronic applications is that the band structure is gapped at E_F, despite the fact that GeTe appears to have always p-type metallic transport properties due to Ge vacancies [29]. Compared to 1SM calculations with ideal α-GeTe(111) stoichiometry presented in Fig. 1(b′), the experimental valence band map in Fig. 1(b) exhibits a rigid shift due to the intrinsic doping as denoted by green arrows. When including an intrinsic p doping in the order of 0.1% in the ground state calculations [Fig. 3(d)], the valence band maximum (VBM) stabilizes with

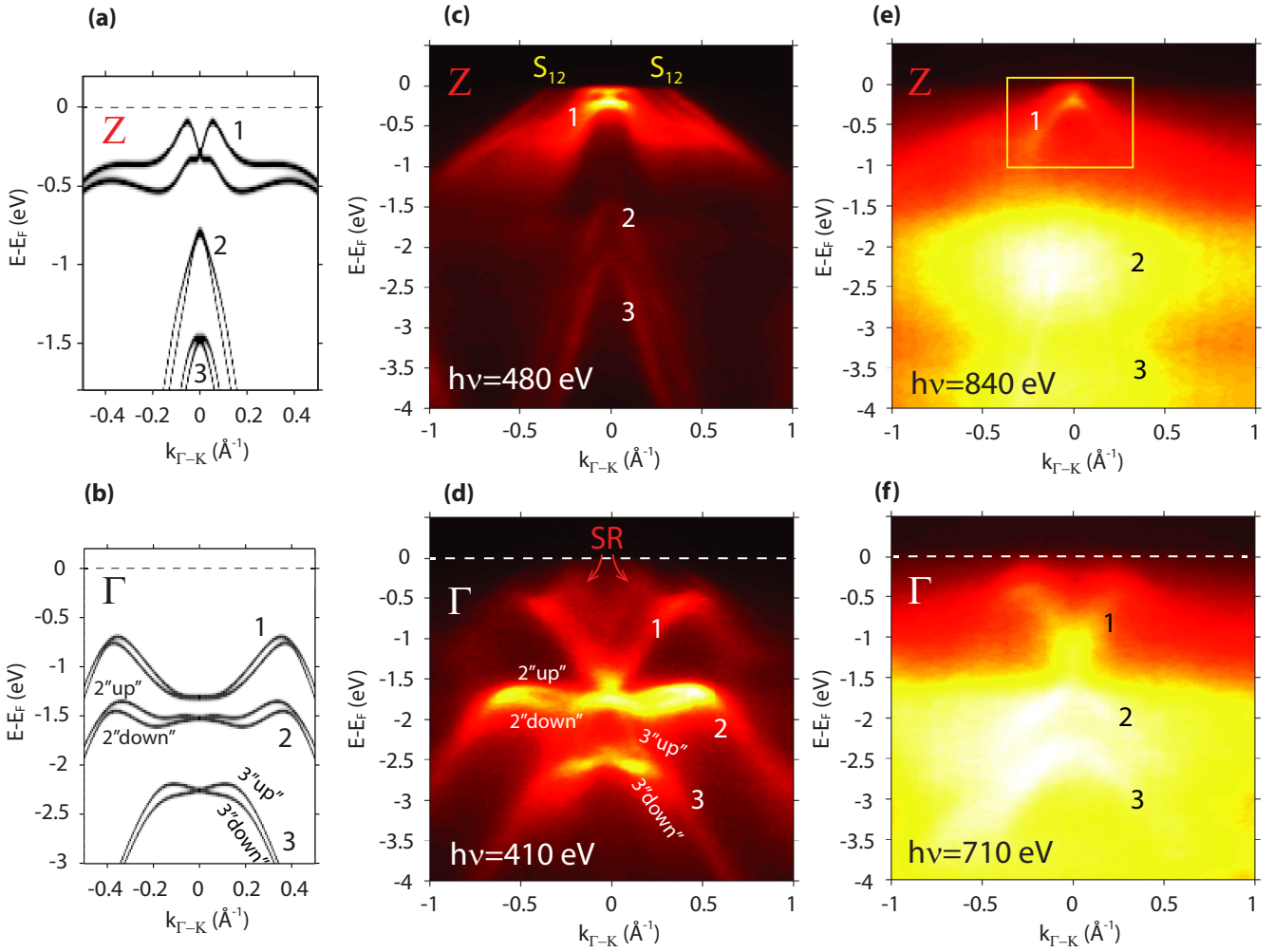

FIG. 2. (a), (b) Bulk α-GeTe(111) ground state calculations along $\overline{\Gamma K}$ at the Γ and Z point, with corresponding soft-X ARPES band maps for uncapped (c), (d) and capped samples (e), (f). The yellow frame in (e) zooms into the bulk Rashba splitting at the Z point (see text).

the narrow gap around 60 meV, in excellent agreement with our experimental data of Fig. 3(c).

Due to the surface sensitivity of ARPES, the experimental band maps cannot be directly compared with bulk band-structure calculations. As seen in Figs. 3(e) and 3(f), the surface electronic structure of the uncapped surfaces significantly differs from the pure bulk as shown in Figs. 3(c) and 3(d). This is due to surface states $S_{1,2}$ localized near the surface, whereas pure bulk states decay toward the surface. However, particular bulk states exist that show a resonantly enhanced spectral weight in the near surface region and degenerate with the bulk at lower binding energy. This is sketched in Fig. 3(h) where the corresponding wave functions are plotted as a function of distance from the surface. Indeed, the integrated intensity calculated for the selected regions in Fig. 3(f) display very different decay lengths [30] characteristic for pure bulk, bulk-derived surface resonance states (SR) and finally pure surface states as presented in Fig. 3(g). The SR include a broad range of states from surface-derived states that are lightly coupled to the bulk continuum; to bulk-derived states that are modulated by the surface potential, as well as bulk states that are altered due to surface band bending. We emphasize that the usual photoemission interpretation that features which disperse with photon energy are *a priori* bulk states is misleading as also bulk-derived SR states show a clear photon-energy dispersion [22,31].

Figure 3(i) shows the momentum distribution curve (MDC) at E_F obtained at $h\nu = 22$ eV for the uncapped surface, color coded with 1SM calculations that reveal the degree of surface localization of the spectral features [22]. Pure surface states with the maximum of their wave functions between the first atomic layer and vacuum are indicated with white-light yellow shading; pure bulk states without surface localization are marked black. They are absent at E_F, but in between the two extreme cases, a variety of SR states with intermediate degree of localization are present.

As seen in Figs. 4(a) and 4(b), all over the Brillouin zone the spectral weight at E_F is formed by these SR states displayed in red color, surrounded by pure surface states marked in yellow (see Supplemental Material [22]). In contrast to Ref. [16], our experimental data indicate that the surface states do not fold back into the occupied states near $\overline{\Gamma}$, meaning their Dirac point lies in the unoccupied region as shown in Fig. 3(f). Thus the soft x-ray ARPES data in Figs. 4(a) and 4(b) elucidate the

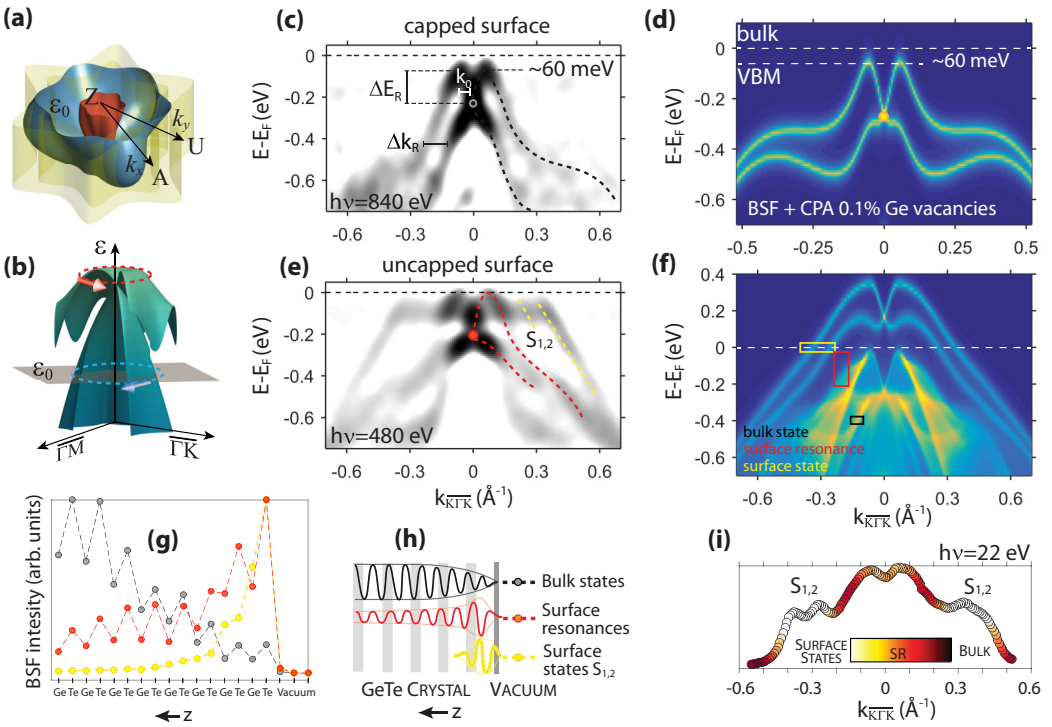

FIG. 3. (a) 3D schematic representation of the 3D bulk spindle torus with intersecting surface states in yellow, at an energy below the Dirac point as seen in the schematic Rashba-split band map in (b). ARPES data (c), (e) and calculations (d), (f) from Te-capped and uncapped α-GeTe(111) surface. (g) BSF intensity decay from selected regions in (f) identifying the surface (yellow), bulk state (black), and surface resonance states (orange-red), schematically depicted in cartoon (h). (i) MDC curve at E_F obtained at $h\nu = 22$ eV; the spectral features are color coded with 1SM calculations (see text).

importance of the bulk-surface resonance in the UV regime where the Z point is located at $h\nu = 22$ eV [22]. In Fig. 4(c) we clearly resolve the bulk states (dashed black lines) and their surface resonance-replica (red dashed lines) shifted up to E_F, as sketched in Fig. 4(d). Similar ARPES data was reported in Ref. [16], however the SR replica was interpreted as a pure bulk state shifted to E_F due to intrinsic α-GeTe(111) p doping. On the contrary, our data indicates that the pure bulk states remain gapped with the same α_R as observed for capped surfaces in Fig. 3(c).

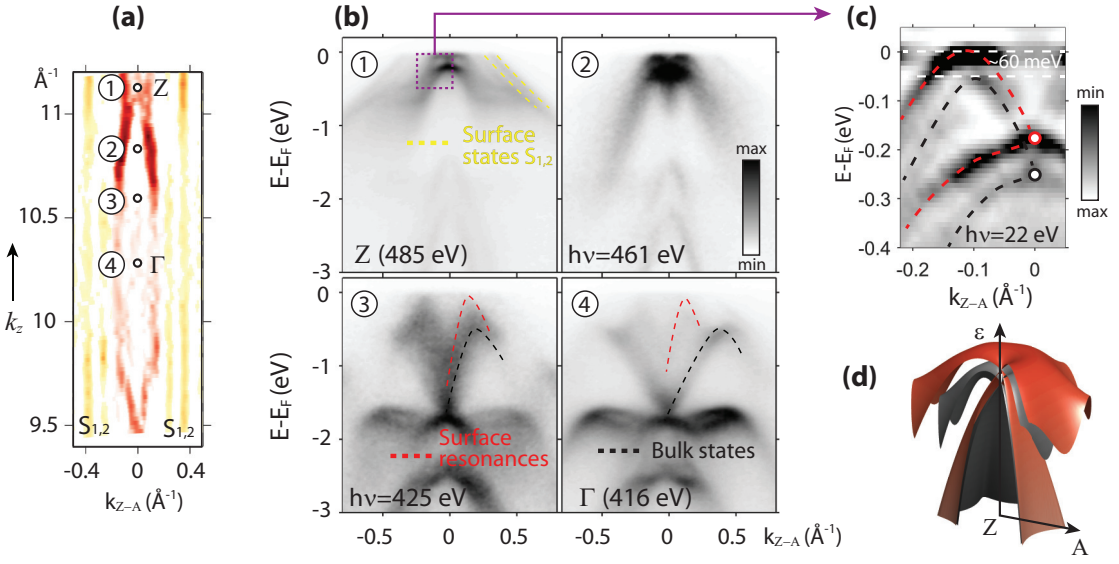

FIG. 4. (a) Second derivative plot of the k_z scan from Fig. 1(c) indicating the surface resonance (red) and pure surface states at E_F (yellow). (b) ARPES maps measured along $\overline{K\Gamma K}$ at four different photon energies the k_z momentum of which is indicated in (a). (c) Second derivative band map at $h\nu = 22$ eV. (d) Schematic representation of the bulk (black) and SR-replica (red) Rashba-split bands.

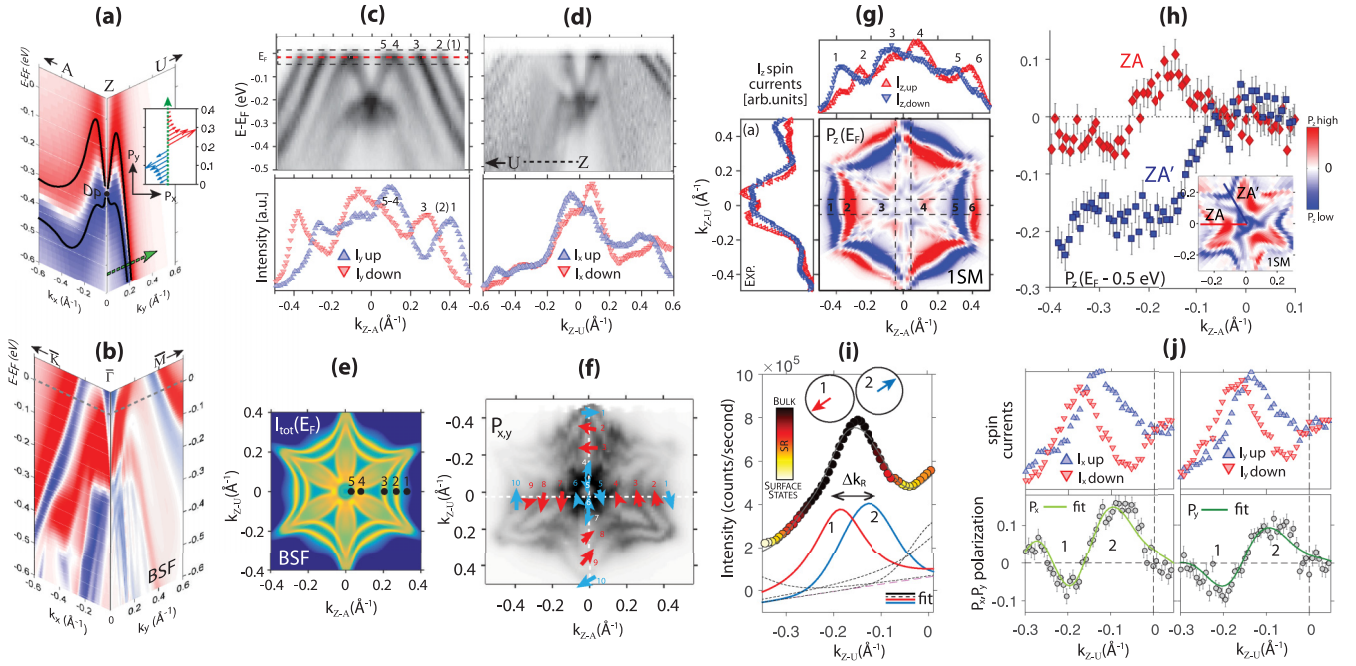

FIG. 5. (a) Bulk and (b) surface spin-resolved BSF with $P_{x,y}$ quiver plot along the green arrow in the inset of panel (a). ARPES data along $\overline{K\Gamma K}$ (c) and $\overline{M\Gamma M}$ (d) with populations of spin-up and spin-down electrons near E_F (bottom panels). (e) Theoretical and (f) experimental Fermi surface map with arrows indicating the spin texture. P_z MDC measured at E_F (g) and below the Dirac point (h), compared with calculations. (i) SARPES data and (j) spin fits of bulk Rashba split bands measured along the Z-U path indicated in (d).

To assess the spin polarization of the individual bands caused by the Rashba effect, SARPES measurements were performed. However, until more efficient spin detection schemes become available [32] we are limited to the UV energy range, precluding the use of Te-capped surfaces. Therefore, all spectral features of the uncapped samples need to be disentangled according to their bulklike or surface-related character. For our SARPES experiments the sample is aligned in such a way that the out-of-plane spin polarization P_z is oriented along the Z-Γ direction and P_x (P_y) along the Z-A (Z-U) directions. SARPES data is visualized as spin-resolved MDCs which we relate to calculations including the surface potential shown in Fig. 5(b); the corresponding spin-integrated Fermi surface map (FSM) is seen in Fig. 5(e).

For analysis of in-plane SARPES at E_F we concentrate on the surface and SR states labeled 1–5 in the band map and MDC depicted in Fig. 5(c). Their appearance is comprehensively described using the vectorial 3D fit [22], and the derived spin texture is summarized in Fig. 5(f). As a whole, the SARPES data suggest an unconventional spin texture with parallel spin orientations different from the simple Rashba model. The altered spin topology can be reconciled via SOC-induced hybridization of the SR and surface states [22]. A similar interband hybridization and spin reorientation has been observed in 2D Rashba systems [33,34]. Since on Te-capped samples the surface states are quenched, the spin topology below E_F reduces into a typical Rashba-like arrangement as seen in Fig. 3(b).

For the out-of-plane spin polarization the band anisotropy between Z-U and Z-A induces a strong hexagonal warping which is responsible for the P_z component [13,35,36]. Here, we concentrate on the P_z spin texture at E_F and below the Dirac point presented in Figs. 5(g) and 5(h), respectively. In order to visualize the complex P_z warping in full extent, calculations are displayed as constant binding energy maps which our MDC data intersect. For the considered MDCs at E_F we unambiguously identify along $\overline{K\Gamma K}$ the antisymmetric peaks 1–6. On the other hand, since the $\overline{M\Gamma M}$ direction is the mirror plane in the α-GeTe(111) crystal structure, the measured P_z polarization should be strictly speaking zero. However, due to the angular resolution limitation indicated by dashed frames in Fig. 5(g), the measured P_z spin polarization is nonzero with clearly symmetric P_z modulation in spin data. The SARPES data measured below the Dirac point along two inequivalent directions $\overline{\Gamma K}$ and $\overline{\Gamma K'}$ and presented in Fig. 5(h) also show excellent agreement with the photoemission calculations and confirm our detailed understanding of the α-GeTe(111) P_z warping around the Z point.

Finally, we address the in-plane $P_{x,y}$ spin polarization below the Dirac point. The ideal locus of $\mathbf{k}$ space momenta for measuring pure bulk-Rashba properties is indicated in Figs. 1(d) and 5(d). The calculations of Fig. 5(a) predict bulk states with distinct canted helicity for the $P_{x,y}$ polarization ($P_x \approx 2P_y$) as indicated by the inset. The corresponding experimental data is summarized in Figs. 5(i) and 5(j). Consistent with the discussion above, we identify the peaks 1–2 as bulk Rashba-split bands with a similar Rashba splitting as for a Te-capped sample along $\overline{\Gamma K}$ [$\Delta k_R(\overline{\Gamma M}) \approx 0.1$ Å^{-1}]. Moreover, their measured canted helicity and Δk_R is consistent with the ground state calculations for which both magnitude and direction of the spin polarization vector traces back to the states from which these electrons originate in the bulk continuum. This is nontrivial especially for systems with large SOC where the total angular momentum is relevant for the

photoemission process rather than only the spin quantum number [37]. Since the measured spin polarization can depend strongly on the final state, the same states were probed with different photon energies [22]. Because the same canted spin arrangement was confirmed in all cases, we conclude that the measured spin signals trace back to initial state bulk Rashba spinors.

In a broader perspective, the unveiled α-GeTe bulk spin structure has far reaching consequences both for fundamental physics and applications. Based on our results, α-GeTe is the prime candidate in manipulatable spin-orbit-driven Rashba physics in 3D **k** space. We emphasize that the giant spin splitting of α_R around 4.2 eVÅ is so far the maximum reported value. Furthermore, for adequately gated capped samples the Fermi surface takes the shape of a single spin polarized spindle torus [38], without additional transport channels. The $\Delta k_R \approx 0.12$ Å^{-1} of the bulk bands translates into a spin precession length of around 1.4 nm, which is two orders of magnitude shorter than what was found for GaAs quantum wells [39], hence favoring ballistic transport in potential device applications. Moreover the α-GeTe Rashba physics extends to the Mn-doped multiferroic $Ge_{1-x}Mn_xTe$ system [19,40]. This opens possibilities towards semiconductors with highly multifunctional properties combining magnetism, ferroelectricity, and Rashba physics for potential device applications.

Constructive discussions with S. Picozzi are gratefully acknowledged. This work was supported by the Swiss National Science Foundation Project No. PP00P2_144742 1. Financial support from the German funding agency DFG (SPP1666 and EB 154/32) and the German ministry BMBF (05K13WMA) is also gratefully acknowledged (H.V., H.E., J.B., and J.M.). G.S. acknowledges support by the Austrian Science Fund, Project P20 550-N20(IR-On). J.M. acknowledges the CEN-TEM Project, Reg. No. CZ.1.05/2.1.00/03.0088, CENTEM PLUS (LO1402) and COST LD15147, co-funded by the ERDF as part of the Ministry of Education, Youth and Sports OP RDI programme. D.K. and V.H. acknowledge the financial support of Czech Science Foundation (Project 14-08124S). F.B. acknowledges the European Community's Seventh Framework Programme (FP7/20072013) under the Grant Agreement No. 290605 (PSI-FELLOW/COFUND).

[1] S. A. Wolf, D. D. Awschalom, R. A. Buhrman, J. M. Daughton, S. von Molnar, M. L. Roukes, A. Y. Chtchelkanova, and D. M. Treger, Science **294**, 1488 (2001).
[2] D. Awschalom and N. Samarth, Physics **2**, 50 (2009).
[3] Y. A. Bychkov and E. I. Rashba, J. Phys. C: Solid State Phys. **17**, 6039 (1984).
[4] S. Datta and B. Das, Appl. Phys. Lett. **56**, 665 (1990).
[5] J. H. Dil, J. Phys.: Condens. Matter **21**, 403001 (2009).
[6] T. Okuda and A. Kimura, J. Phys. Soc. Jpn. **82**, 021002 (2013).
[7] K. Ishizaka, M. S. Bahramy, H. Murakawa, M. Sakano, T. Shimojima, T. Sonobe, K. Koizumi, S. Shin, H. Miyahara, A. Kimura, K. Miyamoto, T. Okuda, H. Namatame, M. Taniguchi, R. Arita, N. Nagaosa, K. Kobayashi, Y. Murakami, R. Kumai, Y. Kaneko, Y. Onose, and Y. Tokura, Nat. Mater. **10**, 521 (2011).
[8] G. Landolt, S. V. Eremeev, Y. M. Koroteev, B. Slomski, S. Muff, T. Neupert, M. Kobayashi, V. N. Strocov, T. Schmitt, Z. S. Aliev, M. B. Babanly, I. R. Amiraslanov, E. V. Chulkov, J. Osterwalder, and J. H. Dil, Phys. Rev. Lett. **109**, 116403 (2012).
[9] C. Martin, E. D. Mun, H. Berger, V. S. Zapf, and D. B. Tanner, Phys. Rev. B **87**, 041104 (2013).
[10] J. S. Lee, G. A. H. Schober, M. S. Bahramy, H. Murakawa, Y. Onose, R. Arita, N. Nagaosa, and Y. Tokura, Phys. Rev. Lett. **107**, 117401 (2011).
[11] G. Landolt, S. V. Eremeev, O. E. Tereshschenko, S. Muff, B. Slomski, K. A. Kokh, M. Kobayashi, T. Schmitt, V. N. Strocov, J. Osterwalder, E. V. Chulkov, and J. H. Dil, New J. Phys. **15**, 085022 (2013).
[12] A. Crepaldi, L. Moreschini, G. Autés, C. Tournier-Colletta, S. Moser, N. Virk, H. Berger, P. Bugnon, Y. J. Chang, K. Kern, A. Bostwick, E. Rotenberg, O. V. Yazyev, and M. Grioni, Phys. Rev. Lett. **109**, 096803 (2012).
[13] D. Di Sante, P. Barone, R. Bertacco, and S. Picozzi, Adv. Mater. **25**, 509 (2013).
[14] S. Picozzi, Front. Phys. **2**, 10 (2014).
[15] M. Wuttig, D. Lusebrink, D. Wamwangi, W. Welnic, M. Gilleszen, and R. Dronskowski, Nat. Mater. **6**, 122 (2007).
[16] M. Liebmann, C. Rinaldi, D. Di Sante, J. Kellner, C. Pauly, R. N. Wang, J. E. Boschker, A. Giussani, S. Bertoli, M. Cantoni, L. Baldrati, M. Asa, I. Vobornik, G. Panaccione, D. Marchenko, J. Sánchez-Barriga, O. Rader, R. Calarco, S. Picozzi, R. Bertacco, and M. Morgenstern, Adv. Mater. **28**, 560 (2016).
[17] H. J. Elmers, R. Wallauer, M. Liebmann, J. Kellner, R. Morgenstern, M. Wang, J. Boschker, R. Calarco, D. Rader, O. Kutnyakhov, S. Chernov, K. Medjanik, C. Tusche, M. Ellguth, H. Volfová, J. Braun, J. Minár, H. Ebert, and G. Schönhense, arXiv:1512.01363.
[18] C. Rinaldi, J. C. Rojas-Sánchez, R. N. Wang, Y. Fu, S. Oyarzun, L. Vila, S. Bertoli, M. Asa, L. Baldrati, M. Cantoni, J.-M. George, R. Calarco, A. Fert, and R. Bertacco, APL Mater. **4**, 032501 (2016).
[19] H. Przybylińska, G. Springholz, R. T. Lechner, M. Hassan, M. Wegscheider, W. Jantsch, and G. Bauer, Phys. Rev. Lett. **112**, 047202 (2014).
[20] V. N. Strocov, T. Schmitt, U. Flechsig, T. Schmidt, A. Imhof, Q. Chen, J. Raabe, R. Betemps, D. Zimoch, J. Krempasky, X. Wang, M. Grioni, A. Piazzalunga, and L. Patthey, J. Synchrotron Radiation **17**, 631 (2010).
[21] M. Hoesch, T. Greber, V. N. Petrov, M. Muntwiler, M. Hengsberger, W. Auwärter, and J. Osterwalder, J. Electron Spectrosc. Relat. Phenom. **124**, 263 (2002).
[22] See Supplemental Material at http://link.aps.org/supplemental/10.1103/PhysRevB.94.205111 for further SARPES data, data analysis, 1-step photoemission calculations, structural characterization and bulk ferroelectricity.
[23] R. T. Lechner, G. Springholz, M. Hassan, H. Groiss, R. Kirchschlager, J. Stangl, N. Hrauda, and G. Bauer, Appl. Phys. Lett. **97**, 023101 (2010).

[24] H. Ebert *et al.* (2014), Munich SPR-KKR package, version 7.2, http://olymp.cup.uni-muenchen.de:/ak/ebert/SPRKKR.
[25] H. Ebert, D. Ködderitzsch, and J. Minár, Rep. Prog. Phys. **74**, 096501 (2011).
[26] V. N. Strocov, M. Kobayashi, X. Wang, L. L. Lev, J. Krempasky, V. V. Rogalev, T. Schmitt, C. Cancellieri, and M. L. Reinle-Schmitt, Synchrotron Radiation News **27**, 31 (2014).
[27] D. J. Singh, J. Appl. Phys. **113**, 203101 (2013).
[28] C. R. Ast, J. Henk, A. Ernst, L. Moreschini, M. C. Falub, D. Pacilé, P. Bruno, K. Kern, and M. Grioni, Phys. Rev. Lett. **98**, 186807 (2007).
[29] A. H. Edwards, A. C. Pineda, P. A. Schultz, M. G. Martin, A. P. Thompson, H. P. Hjalmarson, and C. J. Umrigar, Phys. Rev. B **73**, 045210 (2006).
[30] M.-C. Desjonquères and D. Spanjaard, *Concepts in Surface Physics* (Springer-Verlag, Berlin, Heidelberg, 1993).
[31] S. Kevan, *Angle-Resolved Photoemission: Theory and Current Applications* (Elsevier, Amsterdam, 1992).
[32] V. N. Strocov, V. N. Petrov, and J. H. Dil, J. Synchrotron Radiation **22**, 708 (2015).
[33] H. Bentmann, S. Abdelouahed, M. Mulazzi, J. Henk, and F. Reinert, Phys. Rev. Lett. **108**, 196801 (2012).
[34] B. Slomski, G. Landolt, S. Muff, F. Meier, J. Osterwalder, and J. H. Dil, New J. Phys. **15**, 125031 (2013).
[35] L. Fu, Phys. Rev. Lett. **103**, 266801 (2009).
[36] S. V. Eremeev, G. Landolt, T. V. Menshchikova, B. Slomski, Y. M. Koroteev, Z. S. Aliev, M. B. Babanly, J. Henk, A. Ernst, L. Patthey, A. Eich, A. A. Khajetoorians, J. Hagemeister, O. Pietzsch, J. Wiebe, R. Wiesendanger, P. M. Echenique, S. S. Tsirkin, I. R. Amiraslanov, J. H. Dil, and E. V. Chulkov, Nat. Commun. **3**, 635 (2012).
[37] U. Heinzmann and J. H. Dil, J. Phys.: Condens. Matter **24**, 173001 (2012).
[38] G. Landolt, S. V. Eremeev, O. E. Tereshchenko, S. Muff, K. A. Kokh, J. Osterwalder, E. V. Chulkov, and J. H. Dil, Phys. Rev. B **91**, 081201 (2015).
[39] J. Nitta, T. Akazaki, H. Takayanagi, and T. Enoki, Phys. Rev. Lett. **78**, 1335 (1997).
[40] J. Krempaský, S. Muff, F. Bisti, M. Fanciulli, H. Volfová, A. P. Weber, N. Pilet, P. Warnicke, H. Ebert, J. Braun, F. Bertran, V. V. Volobuev, J. Minár, G. Springholz, J. H. Dil, and V. N. Strocov, Nat. Commun. **7**, 13071 (2016).